Inorg. Chem. **2006**, *45*, 6034–6040

$Na_2[(VO)_2(HPO_4)_2C_2O_4]\cdot 2H_2O$: Crystal Structure Determination from Combined Powder Diffraction and Solid-State NMR

J. F. Colin,[†] T. Bataille,[†] S. E. Ashbrook,[‡,§] N. Audebrand,[†] L. Le Pollès,[†] J. Y. Pivan,[†] and E. Le Fur*[,†]

Sciences Chimiques de Rennes, UMR 6226, CNRS-Université de Rennes 1-ENSCR, 35042 Rennes Cedex, France, and Department of Earth Sciences, University of Cambridge, Downing Street, Cambridge CB2 3EQ, U.K.

Received March 22, 2006

The vanadyl oxalatophosphate $Na_2[(VO)_2(HPO_4)_2C_2O_4]\cdot 2H_2O$ has been synthesized by hydrothermal treatment. Its structure has been determined and refined by combining X-ray powder diffraction and solid-state NMR techniques. It crystallizes with monoclinic symmetry in space group $P2_1$, $a = 6.3534(1)$ Å, $b = 17.1614(3)$ Å, $c = 6.5632(1)$ Å, $\beta = 106.597(1)°$. The structure is related to that of $(NH_4)_2[(VO)_2(HPO_4)_2C_2O_4]\cdot 5H_2O$, which was previously reported. The vanadium phosphate framework consists of infinite $[(VO)(HPO_4)]$ chains of corner-sharing vanadium octahedra and hydrogenophosphate tetrahedra. The oxalate groups ensure the connection between the chains to form a 2D structure. The sodium ions and the water molecules are located between the anionic $[(VO)_2(HPO_4)_2C_2O_4]^{2-}$ layers. The thermal decomposition has been studied in situ by temperature-dependent X-ray diffraction and thermogravimetry. It takes place in three stages, where the first two correspond to water removal and the last to the decomposition of the oxalate group and water elimination, leading to the final product $NaVOPO_4$.

1. Introduction

Ab initio structure determination of inorganic compounds from powder X-ray diffraction remains difficult when single crystals cannot be prepared. The major problem arises from the lack of information due to the projection of the three-dimensional reciprocal space onto a one-dimensional diffraction pattern. Alternative routes using direct-space methods are promising in solid-state chemistry even when there are no organic molecules in the structure. Moreover, the increasing complexity of inorganic materials, combined with larger cell volumes and the possible absence of atomic contrast, may render difficult the process of structure solution from powder diffraction techniques only. Combining structural information from diffraction studies and solid-state NMR spectroscopy has proven to be a good way to assess the structure determination.[1−3]

In this context, the structure determination of the new oxalatophosphate $Na_2[(VO)_2(HPO_4)_2C_2O_4]\cdot 2H_2O$, prepared by hydrothermal treatment, has been performed combining X-ray powder diffraction and multiple-quantum (MQ) MAS ^{23}Na solid-state NMR. The structural model was obtained using direct-space methods, and solid-state NMR studies allowed determination of the actual space group.

Recently, investigations in the vanadium−oxalate−phosphate system have been performed by several research groups. Oxalate compounds are known to be an alternate way to obtain the oxide of interest at low temperature or with large area of the crystal faces that are thought to increase the catalyst activity and selectivity.[4]

These works show two new structural types with 1D and 2D frameworks, respectively. First, a synthesis with piperazine[5] resulted in a one-dimensional vanadium oxalatophosphate framework with monobisdentate oxalate ligands, the other structural type obtained with ammonium,[6] guanidinium,

* To whom correspondence should be addressed. E-mail: eric.le-fur@ensc-rennes.fr. Fax: (+33) 223 238 199. Tel: (+33) 223 238 016.
[†] Université de Rennes.
[‡] University of Cambridge.
[§] Present address: School of Chemistry and EaStCHEM, University of St. Andrews, North Haugh, St. Andrews KY16 9ST, U.K.

(1) Brouwer, D. H.; Darton, R. J.; Morris, R. E.; Levitt, M. H. *J. Am. Chem. Soc.* **2005**, *127*, 10365.
(2) Darton, R. J.; Brouwer, D. H.; Fyfe, C. A.; Villaescusa, L. A.; Morris, R. E. *Chem. Mater.* **2004**, *16*, 600.
(3) Beitone, L.; Huguenard, C.; Gansmüller, A.; Henry, M.; Taulelle, F.; Loiseau, T.; Ferey, G. *J. Am. Chem. Soc.* **2003**, *125*, 9102.
(4) Boudaren, C.; Auffredic, J. P.; Louër, M.; Louër, D. *Chem. Mater.* **2000**, *12*(8), 2324.
(5) Tsai, Y.-M.; Wang, S. L.; Huang, C. H.; Lii, K. H. *Inorg. Chem.* **1999**, *38*, 4183.
(6) Do, J.; Brontchev, R. P.; Jacobson, A. J. *Inorg. Chem.* **2000**, *39*, 3230.

10.1021/ic060483t CCC: $33.50
Published on Web 06/22/2006

ethylenediammonium,[7] and 4,4′-bipyridinium[8] cations resulted in lamellar frameworks built up from bisbidentate oxalate groups connecting infinite vanadophosphate chains. The structure of $Na_2[(VO)_2(HPO_4)_2C_2O_4]\cdot 2H_2O$ is related to these latter compounds.

Thermal decomposition of the title compound has also been studied by combining temperature dependent X-ray diffraction and thermogravimetry techniques, showing a partially reversible dehydration process and a thermal decomposition leading to $NaVOPO_4$.

2. Experimental Section

2.1. Synthesis. A pure blue-green powder of $Na_2[(VO)_2(HPO_4)_2C_2O_4]\cdot 2H_2O$ (**1**) has been obtained by hydrothermal treatment. A mixture of V_2O_5, $Na_2C_2O_4$, H_3PO_4, and H_2O in the molar ratio 1:2:17:170 was introduced in a 23 mL capacity Teflon-lined stainless steel Parr hydrothermal reaction vessel and heated at 120 °C for 3 days. After slowly being cooled to room temperature, the solid was recovered by vacuum filtration, washed with water, and dried in a desiccator. The phase is stable in air and water.

2.2. X-ray Powder Diffraction Data Collection and Structure Determination. High-quality powder diffraction data was obtained employing a Siemens D500 diffractometer with the parafocusing Bragg−Brentano geometry, using monochromatic Cu $K\alpha_1$ radiation ($\lambda = 1.5406$ Å) selected with an incident beam curved-crystal germanium monochromator.[9] To minimize preferred orientation effects, the powder was mounted in a side-loaded sample holder.[10] The pattern was scanned at room temperature, over the angular range 8−120° (2θ), with a step length of 0.02° (2θ) and a counting time of 71 s step^{-1}. The stability of the X-ray source was checked by recording again the diffraction lines at low angles. Powder diffraction data for the monohydrated phase, $Na_2[(VO)_2(HPO_4)_2C_2O_4]\cdot H_2O$, was collected in air at 90 °C with a Bruker AXS D5005 diffractometer using a diffracted-beam-graphite monochromator (Cu $K\alpha_1,\alpha_2$), equipped with a Anton Paar HTK1200 oven camera. The pattern was scanned over the angular range 5−120° (2θ), with a step length of 0.02° (2θ) and a counting time of 57 s step^{-1}. For pattern indexing, the extraction of the peak positions was carried out with the Socabim fitting program available in the PC software package Diffrac^{plus} supplied by Bruker AXS. Pattern indexing was performed with the program DICVOL04.[11] Structure determination was carried out using the parallel tempering algorithm[12] available in the global optimization program FOX.[13] Calculations were performed on a personal computer with a AMD Athlon MP 1700 biprocessor. Structure refinement was achieved with the program FULLPROF[14] available in the software package WINPLOTR.[15] The program DIAMOND (version 2.1e), supplied by Crystal Impact was used for structure drawings.

2.3. Thermal Behavior. Temperature-dependent X-ray diffraction (TDXD) was performed with a powder diffractometer combining the curved-position-sensitive detector from INEL (CPS 120) and a high-temperature attachment from Rigaku. The detector was used in a semifocusing arrangement by reflection (Cu $K\alpha_1$ radiation) as described elsewhere.[16] An angle of 6° was selected between the incident beam and the surface of the sample. The decomposition was carried out, under nitrogen, with a heating rate of 6 °C h^{-1} from room temperature up to 500 °C and of 25 °C h^{-1} up to 600 °C. To ensure satisfactory counting statistics, a counting time of 2700 s per pattern was selected for the thermal decomposition of the precursor. Temperature calibration was carried out with standard materials in the actual temperature range.

Thermogravimetric (TG) measurements were performed with a Rigaku Thermoflex instrument with the same conditions as for TDXD experiment. The powdered sample was spread evenly in large platinum crucibles to avoid mass effects.

Differential scanning calorimetry (DSC) analysis was performed with a TA Q10 instrument. The powdered sample was introduced in an aluminum crucible, sealed, and heated at 10 °C min^{-1} under nitrogen.

2.4. NMR Spectroscopy. ^{23}Na (spin $I = 3/2$) magic-angle spinning (MAS) NMR spectra were recorded on a Bruker ASX 300 spectrometer equipped with a wide-bore 7 T magnet operating at 79.39 MHz for ^{23}Na (spectra not shown) and on a Chemagnetics Infinity 400 spectrometer equipped with a wide-bore 9.4 T magnet operating at 104.3 MHz for ^{23}Na. The sample was packed inside a 4 mm MAS rotor and rotated at speeds up to 12.5 kHz. Two-dimensional triple-quantum MAS spectra were recorded using the *z*-filtered pulse sequence of Amoureux et al.[17] Sign discrimination was restored through the use of the States−Haberkorn−Ruben method. Typical $\omega_1/2\pi$ radio-frequency field strengths employed were ∼150 kHz for the first two pulses and ∼10 kHz for the final pulse. All chemical shifts are referenced to 1 M NaCl(aq), via a secondary reference of NaCl(s) at 7.3 ppm. Any further experimental details may be found in the figure captions. Spectra were simulated using the Dmfit program.[18]

2.5. Magnetic Properties. Magnetic susceptibility measurements were performed on a powdered sample (192.4 mg) from 5 to 300 K in an applied field of 1 kG using a MPMS Quantum Design SQUID magnetometer.

After the data were corrected from diamagnetic contributions, as usual, the $\chi^{-1} = f(T)$ curves were well fitted with a Curie−Weiss law $\chi = C/(T - \theta)$. The magnetic moment obtained from the linear part of the curves ($T \geq 6$ K) is in very good agreement with the expected value for a V^{IV} ion ($\mu_{exp} = 1.68\ \mu_B$, $\mu_{th} = 1.73\ \mu_B$).

2.6. Structure Solution of the Precursor from Powder Diffraction Data and ^{23}Na NMR. Pattern indexing was carried out with the first 20 lines on the basis of a monoclinic solution, with the figures of merit $M_{20} = 54$ and $F_{20} = 116(0.006, 29)$. A least-squares refinement on the resolved diffraction lines available led to the unit-cell dimensions $a = 6.349(1)$ Å, $b = 17.144(3)$ Å, $c = 6.557(1)$ Å, $\beta = 106.59(2)°$, $V = 684.0$ Å^3 [refined zero-shift 0.011° (2θ)]. According to the absence of the reflections $0k0$, $k = 2n + 1$, space groups $P2_1/m$ and $P2_1$ were retained for structure solution. The crystal structure determination was first carried out using the centrosymmetric space group $P2_1/m$.[19] Integrated intensi-

(7) Do, J.; Brontchev, R. P.; Jacobson, A. J. *Chem. Mater.* **2001**, *13*, 2601.
(8) Shi, F.-N.; Almeida Paz, F. A.; Rocha, J.; Klinowski, J.; Trinidade, T. *Inorg. Chim. Acta* **2005**, *358*, 927.
(9) Louër, D.; Langford, J. I. *J. Appl. Crystallogr.* **1988**, *21*, 430.
(10) Swanson, H. E.; Morris, M. C.; Evans, E. H.; Ulmer, L. *Natl. Bur. Stand. (U.S.)* 1964, Monogr. 25, Section 3, 1.
(11) Boultif, A.; Louër, D. *J. Appl. Crystallogr.* **2004**, *37*, 724.
(12) Falcioni, M.; Deem, M. W. *J. Chem. Phys.* **1999**, *110*, 1754.
(13) Favre-Nicolin, V.; Cerny, R. *J. Appl. Crystallogr.* **2002**, *35*, 734.
(14) Rodriguez-Carvajal, J. In *Abstracts of the Powder Diffraction Meeting*; Galy, J.; Louër, D., Eds.; Toulouse, France, 1990; p 127.
(15) Roisnel, T.; Rodriguez-Carvajal, *J. Mater. Sci. Forum* **2001**, *378−381*, 118.
(16) Plévert, J.; Auffrédic, J. P.; Louër, M.; Louër, D. *J. Mater. Sci.* **1989**, *24*, 1913.
(17) Amoureux, J. P.; Fernandez, C.; Steuernagel, S. *J. Magn. Reson. A* **1996**, *123*, 116.
(18) Massiot, D.; Fayon, F.; Capron, M.; King, I.; Le Calvé, S.; Alonso, B.; Durand, J. O.; Bujoli, B.; Gan, Z.; Hoatson, G. *Magn. Reson. Chem.* **2002**, *40*, 70.
(19) Bataille, T.; Mahé, N.; Le Fur, E; Pivan, J.-Y.; Louër, D. *Z. Kristallogr.* **2006**, *23*, 9−14.

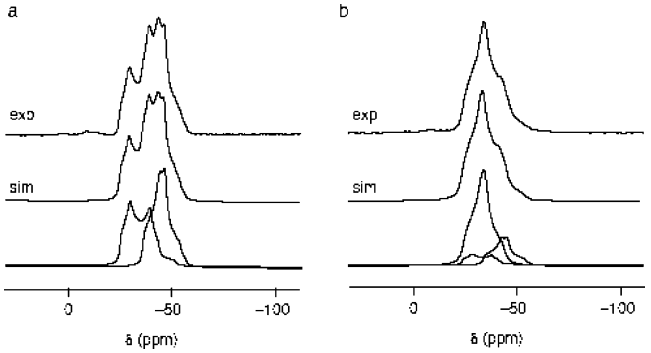

Figure 1. ^{23}Na (104.3 MHz) MAS NMR spectra of $Na_2[(VO)_2(HPO_4)_2C_2O_4]\cdot 2H_2O$, recorded with $B_0 = 9.4$ T and corresponding computer simulated fits for (a) before and (b) after 60 h MAS acquisition. The spectra are the result of averaging 480 transients with a recycle interval of 2 s. The MAS rate was 12.5 kHz. The model spectra were simulated using the parameters, given in Table 1. All chemical shifts are shown relative to 1 M NaCl(aq).

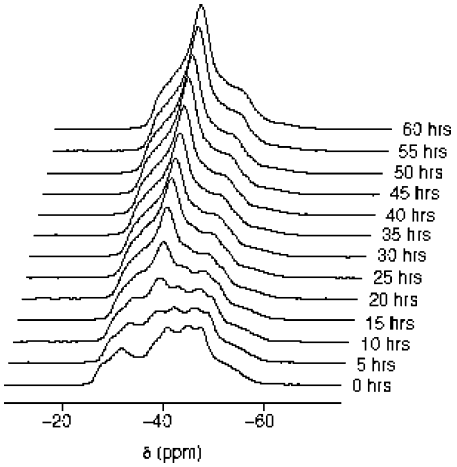

Figure 2. Series of ^{23}Na (104.3 MHz) MAS NMR spectrum of $Na_2[(VO)_2(HPO_4)_2C_2O_4]\cdot 2H_2O$, recorded as a function of time. Each spectrum is the result of averaging 480 transients with a recycle interval of 2 s, with an MAS rate of 12.5 kHz. All chemical shifts are shown relative to 1 M NaCl(aq).

ties were extracted with the program EXPO[20] in the angular range 8−80° (2θ), which includes 187 independent observations among 445 reflections. The intensity set was used for structure solution with the direct methods available in the software. Although several high-electron-density peaks were displayed, which could correspond to V, P, or Na atoms, the expected O atoms located in their environment were not found from subsequent difference Fourier syntheses. Consequently, the heaviest atoms could not be properly attributed to the electron density positions on the lone basis of peak height. The absence of significant preferred orientation allowed starting the structure solution using the parallel tempering algorithm available in FOX. The initial model consisted of one PO_4 tetrahedron, one rigid C_2O_4 group, two free Na atoms, and two water O atoms. The V atom was assumed to be at the center of an octahedron, according to the results reported in the literature.[21] A reasonable solution was found after 4.4 million moves (110 min). One sodium atom needed to be replaced by one water molecule, while the other water molecule was removed from the initial structure model.

^{23}Na (spin $I = 3/2$) NMR spectroscopy is very sensitive to the sodium local environment, both through the chemical shift and the quadrupolar interaction, and allowed us to prove that more than one distinct sodium site existed in the structure. This provides additional constraints to the model defined by X-ray powder diffraction.

Despite the paramagnetic nature of this compound, the ^{23}Na MAS NMR spectrum is clearly dominated by the second-order quadrupolar interaction, resulting in a characteristic powder pattern line shape. The conventional MAS spectrum recorded at 9.4 T, shown in Figure 1a is clearly composed of more than one overlapping sodium signal. As a consequence, *z*-filtered MQMAS experiments[17] were carried out in order to establish unambiguously the number of inequivalent sodium sites in the structure, through the complete removal of the second-order quadrupolar broadening, and to determine their quadupolar interaction parameters (C_Q, η) and isotropic chemical shifts (δ_{iso}).

The sample is stable at ambient temperature over a period of months. It seemed equally stable in a NMR rotor under MAS conditions during the acquisition of the simple 1D ^{23}Na NMR spectrum shown in Figure 1a (a few minutes). However, during the time necessary to acquire a two-dimensional MQMAS spectrum (about 12 h), it appears that a transformation has taken place. Figure 2 shows the evolution of the conventional 1D MAS NMR spectrum as a function of time, over a period of 60 h. After a few hours, the spectrum appears to be dominated by a single new intense resonance superimposed upon the spectrum of the initial phase, as shown in Figure 1b.

It appears, therefore, that the sample is not stable under MAS conditions and slowly decomposes. It is well known that sample heating occurs under MAS conditions, resulting both from the friction due to high-speed rotation and also from RF heating.[22] This temperature elevation under MAS conditions appears to lead to a slow decomposition of $Na_2[(VO)_2(HPO_4)_2C_2O_4]\cdot 2H_2O$. The temperature-dependent X-ray diffraction experiments and the TG analysis established that the dihydrated $Na_2[(VO)_2(HPO_4)_2C_2O_4]\cdot 2H_2O$, stable at ambient temperature, transforms into the monohydrated form at about 65 °C, vide supra. The 2D MQMAS spectra shown in Figure 3, which contains three distinct resonances, can be understood as a superposition of Na signals coming from both the dihydrated (two sodium sites) and monohydrated (one sodium site) phases. Signals labeled 1 and 2 correspond to the two inequivalent sodiums in the dihydrated compound. Quadrupolar coupling constants (C_Q), asymmetry parameters (η) and the quadrupolar product ($P_Q = C_Q\,(1 + \eta^2/3)^{1/2}$) were determined and are given, along with isotropic chemical shifts, in Table 1.

As the NMR spectra of the initial phase clearly show two distinct sodium species (while only one crystallographic site is present in the centrosymmetric structure description) and due to the absence of super structure lines, the structure refinement was then performed with space group $P2_1$. For that, the symmetry-equivalent positions of the framework atoms were generated from these obtained using space group $P2_1/m$. To verify that the previous Na and water O atoms could also be split in two positions in the noncentrosymmetric space group, a difference Fourier synthesis was performed from a partial structure model containing the framework atoms only. Two sodium and two oxygen atoms were clearly evidenced as the four highest peaks in the electron density map, as expected for the space group transformation. They were introduced for completion in the

(20) Altomare, A.; Burla, M. C.; Camalli, M.; Carrozzini, B.; Cascarano, G. L.; Giacovazzo, C.; Guagliardi, A.; Moliterni, A. G. G.; Polidori, G.; Rizzi, R. *J. Appl. Crystallogr.* **1999**, *32*, 339.
(21) Schindler, M.; Hawthorne, F. C.; Baur, W. H. *Chem. Mater.* **2000**, *12*, 1248.
(22) D'Espinose de Lacaillerie, J. B.; Jarry, B.; Pascui, O.; Reichert, D. *Solid State Nucl. Magn. Reson.* **2005**, *28*, 153.

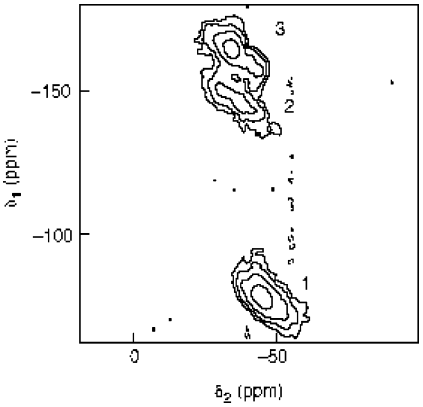

Figure 3. Two-dimensional ^{23}Na (104.3 MHz) triple-quantum MAS NMR spectrum of $Na_2[(VO)_2(HPO_4)_2C_2O_4]\cdot 2H_2O$, recorded using a *z*-filtered pulse sequence. The spectrum is the result of averaging 384 transients with a recycle interval of 2 s for each of 64 t_1 increments of 80 μs (total time ~13 h). The MAS rate was 12.5 kHz. All chemical shifts are shown relative to 1 M NaCl(aq). Three distinct sodium species are observed (denoted 1, 2, and 3). Note, owing to the application of rotor synchronization in t_1, peaks 2 and 3 appear aliased in the δ_1 dimension. Quadrupolar and chemical shift parameters extracted from this (and other similar) spectra are given in Table 1.

Table 1. ^{23}Na NMR Parameters Extracted from MAS and MQMAS Experiments with Estimated Absolute Errors in Parentheses

compound	C_Q (MHz)	η	P_Q (MHz)	δ_{iso} (ppm)
$Na_2[(VO)_2(HPO_4)_2C_2O_4]\cdot 2H_2O$	1.8(±0.1)	0.7(±0.1)	2.0(±0.1)	−36(±2)
$Na_2[(VO)_2(HPO_4)_2C_2O_4]\cdot 2H_2O$	2.2(±0.1)	0.3(±0.1)	2.2(±0.1)	−22(±2)
$Na_2[(VO)_2(HPO_4)_2C_2O_4]\cdot H_2O$	1.75(±0.1)	0.9(±0.1)	2.0(±0.1)	−26(±2)

Rietveld refinement in the angular range 8−120° (2θ). A pseudo-Voigt function was used for the individual line profiles, and the usual quadratic function in tan θ (known as the Caglioti function) was selected to characterize the angular dependence of peak widths. The background was described with a linear interpolation between refined intensity points. Soft restraints were applied on distances within PO_4 and C_2O_4 groups. While the structure refinement converged to a satisfactory structure model, negative isotropic atomic displacement parameters were observed for many atoms. The porous nature of the surface of the powder, combined with the layered crystal structure of the compound, is the reason a surface roughness was observed after the preparation of the sample for data collection. It is known that this feature greatly influences the microabsorption effect, which is responsible for a considerable decrease in diffraction line intensities, especially at low angles.[23] In the Rietveld refinement, it is reflected by rather low or negative isotropic atomic displacement parameters.[23] Then, two parameters used for correction of microabsorption were refined (eq 17 from ref 23). In addition, isotropic atomic displacement parameters were allowed to vary in the same manner for atoms of the same species within a molecule, in the wide range 0.5−3.5 Å^2. Details of the Rietveld refinement are given in Table 2. Figure 4 shows the final fit between observed and calculated patterns. Bond distances and angles are displayed in Table 3.

3. Results and Discussion

3.1. Structure Description. The structure of **1** is related to that of $(NH_4)_2[(VO)_2(HPO_4)_2(C_2O_4)]\cdot 5H_2O$ previously reported by Do et al.[6] In **1**, each vanadium atom and phosphorus atom occupies two crystallographically unique

(23) Pitschke, W.; Hermann, H.; Mattern, N. *Powder Diffr.* **1993**, *8*, 74.

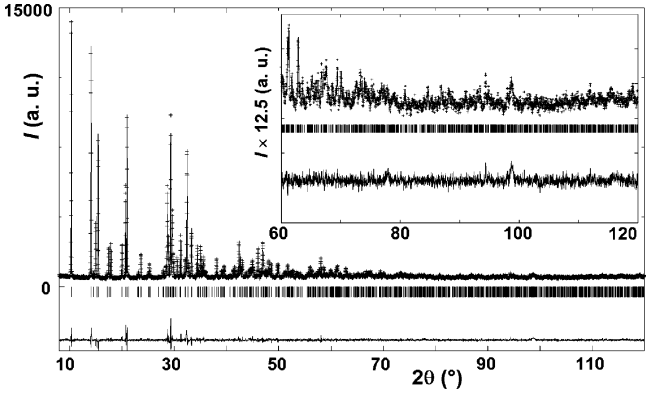

Figure 4. Final fit between observed and calculated patterns for $Na_2[(VO)_2(HPO_4)_2(C_2O_4)]\cdot 2H_2O$.

Table 2. Crystallographic Data and Details of the Rietveld Refinement for $Na_2[(VO)_2(HPO_4)_2(C_2O_4)]\cdot 2H_2O$

empirical formula	$C_2H_6Na_2O_{16}P_2V_2$
fw, g/mol	495.87
cryst syst	monoclinic
space group	$P2_1$ (No. 4)
a, Å	6.3534(1)
b, Å	17.1614(3)
c, Å	6.5632(1)
β, deg	106.597(1)
V, Å^3	447.55
Z	2
wavelength, Å	1.5406
2θ range, deg	8−120
no. of atoms	24
no. of reflns	1109
no. of structural params	83
no. of profile params	26
no. of restraints	32
R_F	0.055
R_B	0.052
R_p	0.044
R_{wp}	0.058
R_{exp}	0.038

positions. The vanadium atom is coordinated by six oxygen atoms, forming a distorted octahedron. Three of the oxygen atoms are shared with three PO_3OH groups with typical distances ranging from 1.91(4) to 2.17(3) Å. Two of the remaining oxygen atoms are shared with a C_2O_4 group (d_{V-O} = 1.97(2)−2.32(2) Å). The last oxygen atom has a significantly shorter V=O bond length corresponding to the vanadyl group ($d_{V=O}$ = 1.49(3) and 1.79(3) Å). Three of the oxygen atoms in the tetrahedral PO_3OH group are shared with vanadium atoms (d_{P-O} = 1.46(3)−1.55(3) Å), and the fourth oxygen atom is terminal with a longer P−O distance, (d_{P-OH} = 1.51(2) and 1.67(2) Å), indicative of the P−OH group. Three vanadium octahedra are linked together by a PO_3OH group to form infinite chains $[VOHPO_4]_\infty$. The infinite chains are connected to each other by C_2O_4, resulting in layers with the formula $[(VO)_2(HPO_4)_2(C_2O_4)]^{2-}$, as shown in Figure 5a.

The Na^+ species, as well as water molecules, are located in the space between the $[(VO)_2(HPO_4)_2(C_2O_4)]$ layers (Figure 5b). Two distinct sodium atoms corresponding to the structural information given by the solid-state NMR experiments are present. They possess closely related environments (Figure 6): one oxygen atom comes from the vanadyl groups (O2), one is shared between a vanadium atom

Table 3. Selected Distances (Å) and Bond Angles (deg) for $Na_2[(VO)_2(HPO_4)_2(C_2O_4)]\cdot 2H_2O$

	VO_6 Octahedra		
V1−O1	1.49(3)	V2−O2	1.79(3)
V1−O12^{i}	1.91(4)	V2−O11	1.98(3)
V1−O21	2.08(3)	V2−O14^{iii}	2.17(3)
V1−O24^{ii}	1.91(3)	V2−O22^{iv}	2.02(4)
V1−O32	2.11(2)	V2−O31	1.97(2)
V1−O41	2.12(2)	V2−O42^{iv}	2.32(2)
	PO_4 Tetrahedra		
P1−O11	1.48(3)	P2−O21	1.46(3)
P1−O12	1.55(3)	P2−O22	1.47(3)
P1−O13	1.67(2)	P2−O23	1.51(2)
P1−O14	1.48(3)	P2−O24	1.50(3)
	C_2O_4 Group		
C1−O31	1.28(2)	C2−O41^{vi}	1.24(2)
C1−O32^{v}	1.28(2)	C2−O42^{iv}	1.29(2)
C1−C2	1.58(2)		
	Sodium Environment		
Na1−O2	2.74(3)	Na2−O1	2.47(3)
Na1−O13^{iii}	2.74(3)	Na2−O2	2.76(3)
Na1−O22	2.41(3)	Na2−O12	2.50(3)
Na1−O31	2.53(2)	Na2−O21^{iv}	2.90(3)
Na1−O42	2.36(2)	Na2−O32	2.39(2)
Na1−Ow1	2.49(4)	Na2−O41	2.32(2)
		Na2−Ow2	2.30(2)
	Water Molecules		
Ow1···O13	2.60(4)	Ow2···O23	2.91(3)
Ow1···O14^{i}	2.51(4)	Ow2···O24^{iv}	2.99(3)
Ow1···O42^{ii}	2.97(4)	Ow2···O32	2.90(3)
Ow1···Ow2^{v}	2.87(4)		
	VO_6 Octahedra		
O1−V1−O12^{i}	109(3)	O2−V2−O11	98(2)
O1−V1−O21	95(2)	O2−V2−O14^{iii}	100(2)
O1−V1−O24^{ii}	99(2)	O2−V2−O22^{iv}	98(2)
O1−V1−O32	84(2)	O2−V2−O31	104(2)
O1−V1−O41	163(2)	O2−V2−O42^{iv}	176(2)
O12^{i}−V1−O21	88(2)	O11−V2−O14^{iii}	161(2)
O12^{i}−V1−O24^{ii}	93(2)	O11−V2−O22^{iv}	92(2)
O12^{i}−V1−O32	166(2)	O11−V2−O31	89(2)
O12^{i}−V1−O41	84(2)	O11−V2−O42^{iv}	85(2)
O21−V1−O24^{ii}	164(2)	O14^{iii}−V2−O22^{iv}	89(2)
O21−V1−O32	86(2)	O14^{iii}−V2−O31	82(2)
O21−V1−O41	74(1)	O14^{iii}−V2−O42^{iv}	76(1)
O24−V1−O32	90(2)	O22^{iv}−V2−O31	157(2)
O24−V1−O41	90(2)	O22^{iv}−V2−O42^{iv}	84(2)
O32−V1−O41	82(1)	O31−V2−O42^{iv}	73(1)
	PO_4 Tetrahedra		
O11−P1−O12	107(3)	O21−P2−O22	117(3)
O11−P1−O13	102(2)	O21−P2−O23	114(3)
O11−P1−O14	105(3)	O21−P2−O24	111(3)
O12−P1−O13	112(3)	O22−P2−O23	99(3)
O12−P1−O14	112(3)	O22−P2−O24	111(3)
O13−P1−O14	117(2)	O23−P2−O24	102(2)
	C_2O_4 Group		
O31−C1−O32^{v}	128(2)	O41^{vi}−C2−O42^{iv}	130(2)
O31−C1−C2	112(2)	O41^{vi}−C2−C1	116(2)
O32^{v}−C1−C2	120(2)	O42^{iv}−C2−C1	114(2)

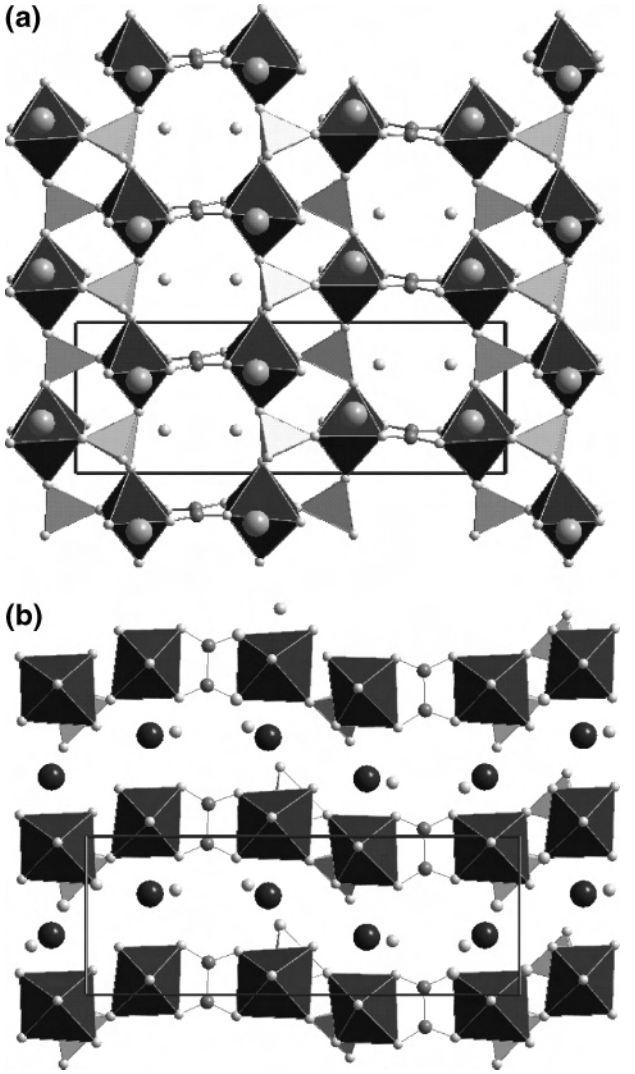

Figure 5. Views of **1**, (a) along the [001] and (b) along the [100]. Vanadium polyhedra are in dark gray, phosphate polyhedra in light gray, sodium atoms are in black, and interlayer water molecules and oxygen atoms are in white.

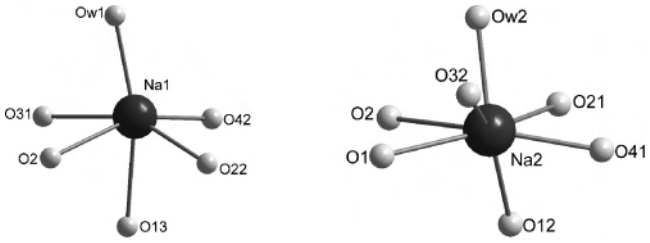

Figure 6. Environment of the two crystallographic sodium atoms.

and a phosphorus atom (O22 and O21 for Na1 and Na2, respectively), and two other oxygen atoms are shared between vanadium and carbon atoms (O31 and O42 for Na1, O41 and O32 for Na2), thus forming the basal plane of a square pyramid, while the water molecules occupy the apical position of the polyhedra (Ow1 and Ow2, respectively). For Na1, a trans oxygen atom (O13) from a POH group leads to a distorted octahedron. For Na2, two other oxygen atoms arising from a vanadyl group and a vanadium phosphorus bridge (O1 and O12, respectively) generate, together with the five other oxygen atoms, a complex geometry. The differences between the two sodium atoms may arise from a displacement of the Na2 atom from the center of the octahedron.

According to the formula of **1**, the oxidation state for the vanadium atoms is +4, but some vanadium oxygen distances observed in the structure (cf. Table 3) differ significantly from the values generally observed for V^{4+} compounds as reported by Schindler et al.[21] Indeed, for V^{4+} atoms in octahedral coordination, bond lengths fall in the range 1.48−1.74 Å for vanadyl V=O bonds, 1.86−2.16 Å for equatorial bonds, and 2.00−2.56 Å for trans bonds. From the studies

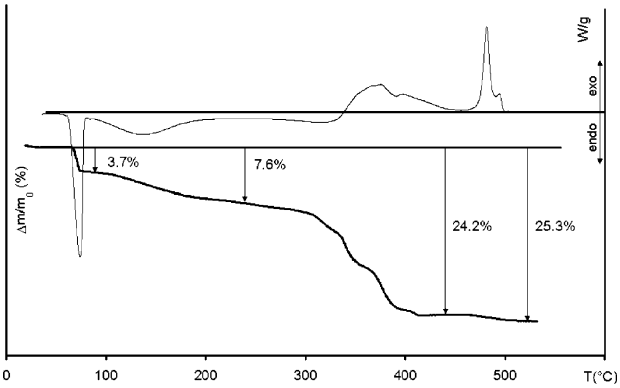

Figure 7. DSC (above) and TG (below) curves for $Na_2[(VO)_2(HPO_4)_2(C_2O_4)]\cdot 2H_2O$.

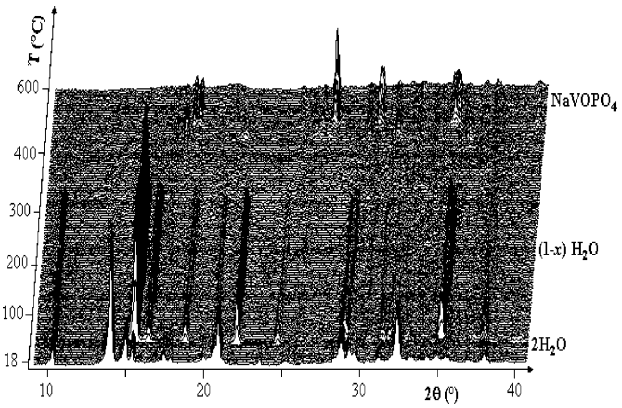

Figure 8. Temperature-dependent X-ray powder diffraction of $Na_2[(VO)_2(HPO_4)_2(C_2O_4)]\cdot 2H_2O$.

of Schindler, the observed vanadium−oxygen bond distances for the two vanadium atoms in **1** are consistent with V^{4+} species. All the V−O bonds reported[21] for the V^{3+} are in the range 1.88−2.16 Å, which rules out the possibility of V^{3+} in the structure of **1**. The bond valence sum calculations[24] result in incorrect values for the two vanadium ions (V1 = 4.90, V2 = 3.29), but the mean value of 4.1 is in good agreement with the expected value of 4. This observation is confirmed by the magnetic data which give a magnetic moment per vanadium ion of 1.68 μ_B, very close to the expected V^{4+} value of 1.73 μ_B, vide infra. For a mixed V^{3+}/V^{5+}-containing compound, the experimental magnetic moment for the V^{3+} would be 2.45 μ_B, which clearly differs from the theoretical value of 2.83 μ_B.

3.2. Thermal Decomposition. The thermal behavior of the mixed oxovanadium sodium oxalate phosphate has been investigated under nitrogen using thermogravimetry, differential scanning calorimetry (Figure 7), and X-ray thermodiffractometry (Figure 8). The thermal decomposition can be described as a three-step process. The initial weight loss (∼3.7%) observed between ∼65 and ∼75 °C corresponds to the departure of one water molecule (calculated weight loss: 3.6%). It is attributed to one weakly bound water molecule located between the layers of the structure. The dehydration process is associated with an endothermic peak at ∼65 °C on the DSC curve and a structural change seen on the TDXD plot at ∼60 °C. The powder diffraction pattern of the intermediate monohydrate has been recorded in situ at 90 °C in air with a D5005 diffractometer. Indexing of the pattern led to a monoclinic unit cell, with the following refined parameters: $a = 6.3887(5)$ Å, $b = 17.097(2)$ Å, $c = 5.9255(5)$ Å, $\beta = 106.130(7)°$, $V = 621.7$ Å^3 [$M_{20} = 41$; $F_{20} = 79(0.008, 31)$] [refined zero-shift 0.027° (2θ)]. The systematic absence of the $0k0$: $k = 2n + 1$ reflections suggest the space groups $P2_1$ and $P2_1/m$. NMR studies showing only one sodium line indicate that the correct space group is the centrosymmetric one. Structure determination was attempted using various strategies but did not succeed due to the relatively low quality of the diffraction data of this decomposition product. Nevertheless, the weak contraction of the unit cell parameters suggests a topotactic process for the dehydration. Furthermore, a complementary thermogravimetry experiment up to 100 °C, followed by a cooling to room temperature, demonstrated that the first dehydration step is fully reversible. The second weight loss (exptl/calcd: ∼7.6/7.2%) starting at about 100 °C is associated with a DSC endothermic peak at about 115 °C. It is consistent with the departure of the second water molecule, also located between the layers. While the weight loss is continuous, the framework of the structure is maintained until ∼340 °C since no structural change appears on the TDXD plot (Figure 8). Between 340 and ∼395 °C, an amorphous state is observed. It corresponds to the decomposition of the oxalate group, thus leading to the structure collapse. The decomposition is complex, as shown by the three inflections at about 325, 355, and 395 °C on the TG curve. They agree well with the successive exothermic peaks which are observed in the range 330−390 °C. The TDXD plot shows at about 395 °C the emergence of the diffraction lines of an unidentified compound stable until ∼455 °C (weight loss: 24.2%). The crystallization is confirmed by an exothermic peak at ∼480 °C. The last weight-loss of ∼25.3% agrees well with that corresponding to the formation of $NaVOPO_4$ (calcd: 25.4%) whose diffraction lines appear at about 455 °C (PDF2 no. 76-0417[25]).

4. Conclusion

The structure of $Na_2[(VO)_2(HPO_4)_2C_2O_4]\cdot 2H_2O$, prepared by hydrothermal treatment, has been solved combining X-ray powder diffraction and ^{23}Na solid-state NMR. The structure was solved, at first, by X-ray powder diffraction using direct-space methods in the centrosymmetric space group $P2_1/m$. The combination of the absence of superstructure lines in XRD experiments and the observation of two inequivalent sodium sites by NMR leads to the correct space group $P2_1$. Therefore, the information provided by both powder XRD and NMR was necessary to ascertain the actual space group.

The thermal properties have been investigated using TG and thermal-dependent X-ray diffraction. Three steps of decomposition are observed with, first, a topotactic dehydration process then oxalate decomposition leading to $NaVOPO_4$ at 450 °C.

(24) Brown, I. D.; Altermatt, D. *Acta Crystallogr.* **1985**, *B41*, 244.

(25) International Centre for Diffraction Data, Newtown Square, PA.

Acknowledgment. The authors thank G. Marsolier for his assistance in powder X-ray diffraction data collection and T. Guizouarn for magnetic susceptibility measurement. The spectrometer in Cambridge was supported by an infrastructure grant (JIF 2000) from UK HEFCE (GR/65557).

Supporting Information Available: Crystallographic data. This material is available free of charge via the Internet at http://pubs.acs.org.

IC060483T